PAPER

Check for updates

A PVP-stabilized cerium oxide–platinum nanocomposite synthesized in TEG: pro-/antioxidant activities †

Nadiia M. Zholobak, *ab Iryna V. Dubova, a Anastasiia Deineko, c
Viacheslav Kalinovych, c Jaroslava Nováková, c Iva Matolínová, c
Kevin C. Prince, cd Tomáš Skála, c Alexander B. Shcherbakov a
and Nataliya Tsud c

Cerium oxide nanoparticles (CeNPs) represent a highly promising material for a number of chemical and biological applications involving oxidation–reduction processes. However, the impact of synthesis conditions, as well as the incorporation of synergistic agents of a different catalytic nature, on the antioxidant or prooxidant properties of CeNPs remains a subject of ongoing investigation. In this study, non-stoichiometric CeNPs ($\sim$10% Ce^{3+}) stabilized by polyvinylpyrrolidone (PVP) were synthesized through the thermal autoxidative decomposition of cerium(III) nitrate in a high-boiling glycol. A novel approach for the synthesis of CeNPs in the absence of additives (PVP-CeNPs) and with platinum (PVP-CeNPs–Pt), followed by the formation of platinum nanoparticles (PVP-PtNPs), was employed in a stepwise one-pot process. In chemical tests, the PVP-CeNPs–Pt nanocomposite exhibited enhanced peroxidase-mimicking activity and accelerated the Fenton-type reaction of dye decolorization. Nevertheless, it was found to have the ability to reduce adrenaline autoxidation *via* the superoxide dismutase-mimicking pathway. *In vitro* studies demonstrated that PVP-CeNPs and PVP-CeNPs–Pt enhanced H_2O_2-induced oxytosis while restoring cellular metabolic activity inhibited by the Fenton-like pathway of cellular apoptosis (ferroptosis) initiated by sulfasalazine. The authors suggest that the oxidoreductase activity of CeNP-based systems in the chemical tests and in biological processes *in vitro* may be caused by different mechanisms, which are discussed.

Introduction

Pro- and antioxidant nanomaterials are expected to play an important role in next-generation theranostics.[1] While current knowledge provides an abundance of such materials, a more in-depth investigation of the mechanisms of action and methodologies associated with these mechanisms is required to highlight the most relevant ones through targeted synthesis.

Cerium oxide nanoparticles (CeNPs) have been shown to act as oxidoreductase mimetics in both inanimate and biological systems, scavenging a range of reactive oxygen species (ROS) or enhancing ROS activities. This compound exhibits functional

similarities to a number of oxidoreductases, including catalase, peroxidase, oxidase, and superoxide dismutase (SOD) enzymes. It also has the ability to scavenge free radicals, including oxygen-associated ones such as hydroperoxyl and hydroxyl radicals.[2–6] At the same time, the behavior of these nanoparticles is significantly influenced by their morphology, which in turn depends on the synthesis methods used, resulting in a certain habitus and stoichiometry of CeNPs.[5,6] In addition, further research is needed to determine the influence of different coating agents on the properties of nanomaterials. For instance, CeNPs regulate aquaporin functionality by increasing permeability to water and H_2O_2, and polyacrylate capping has a pronounced effect on this activity, influencing the pro- or antioxidant properties of CeNPs.[7] This complex interaction deserves further investigation.

Similarly, platinum nanoparticles (PtNPs) exhibit extensive antioxidant properties, including the ability to mimic the functions of SOD, catalase, and peroxidase. In some cases, they have shown greater efficacy than their natural enzyme counterparts.[8] Ye *et al.* demonstrated that polyvinylpyrrolidone (PVP)-capped Pt nanocubes were efficiently used as peroxidase nanozymes, exhibiting the ability to efficiently reduce ROS

aZabolotny Institute of Microbiology and Virology, National Academy of Sciences of Ukraine, Zabolotny Street 154, Kyiv, 03680, Ukraine. E-mail: n.zholobak@gmail.com

bKyiv National University of Technologies and Design, Mala Shyianovska Street 2, Kyiv, 01011, Ukraine

cCharles University, Faculty of Mathematics and Physics, Department of Surface and Plasma Science, V Holešovičkách 2, Prague, 18000, Czech Republic

dElettra-Sincrotrone Trieste S.C.p.A., Area Science Park, Strada Statale 14 km 163.5, Basovizza, Trieste, 34149, Italy

levels *in vitro* and fully restore physiological cellular homeostasis.[9] PVP-functionalized PtNPs have been demonstrated to catalyze the decomposition of H_2O_2 generated by the autoxidation of hydroquinone, thereby protecting organic substances under oxidative conditions.[10] Polyacrylic acid-stabilized PtNPs have been shown to inactivate peroxyl and DPPH radicals and to inhibit linoleic acid peroxidation.[11] PtNPs have been shown to quench hydrogen peroxide and superoxide anion radicals[12] with minimal or no cytotoxicity.[13] Apoferritin-encapsulated PtNPs have been shown to exhibit both catalase and peroxidase-like activity,[14] which effectively reduces oxidative stress in cells and enhances cell viability.[15] The anti-inflammatory potential of Pt nanozymes has been demonstrated[16] and a comparative study showed that both platinum and cerium oxide NPs can protect cells from oxytosis.[17]

Ceria-supported platinum is a well-established material with a number of technical applications, including oxidation–reduction processes.[18–21] For example, it has been used in three-way catalysts for many years.[20,21] Unfortunately, there is a very limited amount of data on the combined use of platinum and cerium oxide NPs in biological systems with respect to oxidoreductase activity. For example, the presence of Pt clusters on the surface of CeNPs has been demonstrated to enhance their oxidase activity, thereby increasing the efficacy of tumor treatment.[22] CeNPs decorated with single Pt atoms have been shown to possess durable antioxidant catalytic activity with 3–10 times higher efficacy than CeNPs. This makes them an optimal choice for the non-invasive treatment of neurotrauma, which can significantly improve wound healing and reduce neuro-inflammation.[23] Pt/cube-CeO_2 nanocomposites have shown enhanced peroxidase activity with promising potential for applications in diagnostics, biomedicine and environmental remediation.[24]

This study investigates the effect of Pt nanoparticles on the physicochemical and biological properties of PVP-stabilized CeNPs. The formation of the system was performed in a stepwise manner: first nucleation of PtNPs, followed by synthesis of CeNPs on top, resulting in a PtNP (2 wt% Pt) surrounded by self-assembled CeNPs. The prepared systems were characterized by UV-vis spectrophotometry, transmission electron microscopy (TEM), and X-ray photoelectron spectroscopy (XPS). The synergistic mode of action of bare CeNPs, PtNPs and platinum-containing nanocomposites in the interaction with ROS in chemical and biological processes was investigated. The known morphology of the nanocomposite allowed us to evaluate the combined effect of the oxidoreductase action in the context of the activity of each type of nanoparticles, thereby clarifying the differences in their working mechanisms. In the studied systems, the interplay of the electronic properties of the system components is minimized because the close contact of the nanoparticles is prevented by the PVP shell. The effects of the PVP-CeNPs and PVP-CeNPs–Pt systems on oxytosis *in vitro* were found to be consistent with their enzymatic properties in chemical assays, in contrast to the iron-dependent oxytosis process that occurs *via* the Fenton-like mechanism, known as ferroptosis.

Results and discussion

Synthesis of PVP-CeNPs, PVP-PtNPs, and PVP-CeNPs–Pt

TEG is a liquid higher glycol and high boiling-point solvent. When heated in a TEG medium, cerium(III) nitrate disproportionately decomposes into cerium(IV) oxide nanoparticles, see Fig. 1(b). Glycols enable the formation of ultra-small CeNPs by acting as excellent complexing agents for cerium ions. At the same time, glycols (especially ethylene glycol) are good media and reducing agents for the synthesis of noble metal NPs, where PVP is used as a capping and stabilizing agent.[25] This allows the stepwise preparation of PVP-CeNPs–Pt nanocomposites in a single pot. The proposed process is easy to perform and does not require any special equipment, except a fume hood due to the production of harmful nitrogen oxides. The sequence of steps and the appearance of the systems are shown in Fig. S1 of the ESI.† The resulting TEG sols were transferred to an aqueous medium by long-term dialysis against water (240 h), where PVP prevents the agglomeration of NPs in water.

Characterization of PVP-CeNPs, PVP-PtNPs, and PVP-CeNPs–Pt

UV-vis spectroscopy. The UV-vis spectra of pristine PVP-CeNPs, PVP-PtNPs, and PVP-CeNPs–Pt nanocomposites after dialysis are shown in Fig. 1(c). A characteristic band of Ce^{4+} at 296–298 nm is observed, and it can be seen that the presence of Pt (2 wt%) in the PVP-CeNPs–Pt nanocomposite has little effect on the absorption spectrum.

TEM analysis. TEM micrographs of the synthesized nanocomposites are shown in Fig. 2(a–c); polyol-mediated CeNPs were found to be very small, about 2 nm in size. Platinum nanoparticles synthesized by the TEG method in the presence of PVP have cubic and octahedral shapes and size less than 20 nm, similar to nanoparticles obtained by the EG method.[26] The presence of platinum nanoparticles during the synthesis of the PVP-CeNPs–Pt nanocomposite does not affect the ceria habitus, but only the arrangement—a substantial part of the CeNPs appears to surround the Pt NPs (see Fig. 1(a) and 2(c)).

XPS analysis. XPS data of the synthesized nanoparticles are shown in Fig. 2, bottom. The Ce 3d core level is typical for partially reduced cerium oxide with contributions from Ce^{4+} and Ce^{3+} states. The average oxide stoichiometry calculated from the area of the Ce 3d component was estimated to be $CeO_{1.95}$ for PVP-CeNPs and PVP-CeNPs–Pt. The O 1s core level is similar for these two samples containing lattice O_L and adsorbed hydroxyl (water) OH^- (H_2O) components. For PVP-PtNPs, the oxygenated carbon species CO is also expected to contribute an O 1s signal at the same energy as the OH^- peak, while the H_2O component has the highest intensity. The significant water signal reflects the longer drying time for PVP-PtNPs compared to cerium oxide containing systems. Two components were identified in the Pt 4f core level: metallic Pt^0 and partially oxidized $Pt^{\delta+}$.[27] The relative concentrations of the different Ce and Pt species for all nanocomposites, calculated from the corresponding areas of the XPS signals, are summarized in Table 1. Thus, the Pt 4f spectra confirm the presence of oxidized platinum in the NPs with a 20% higher
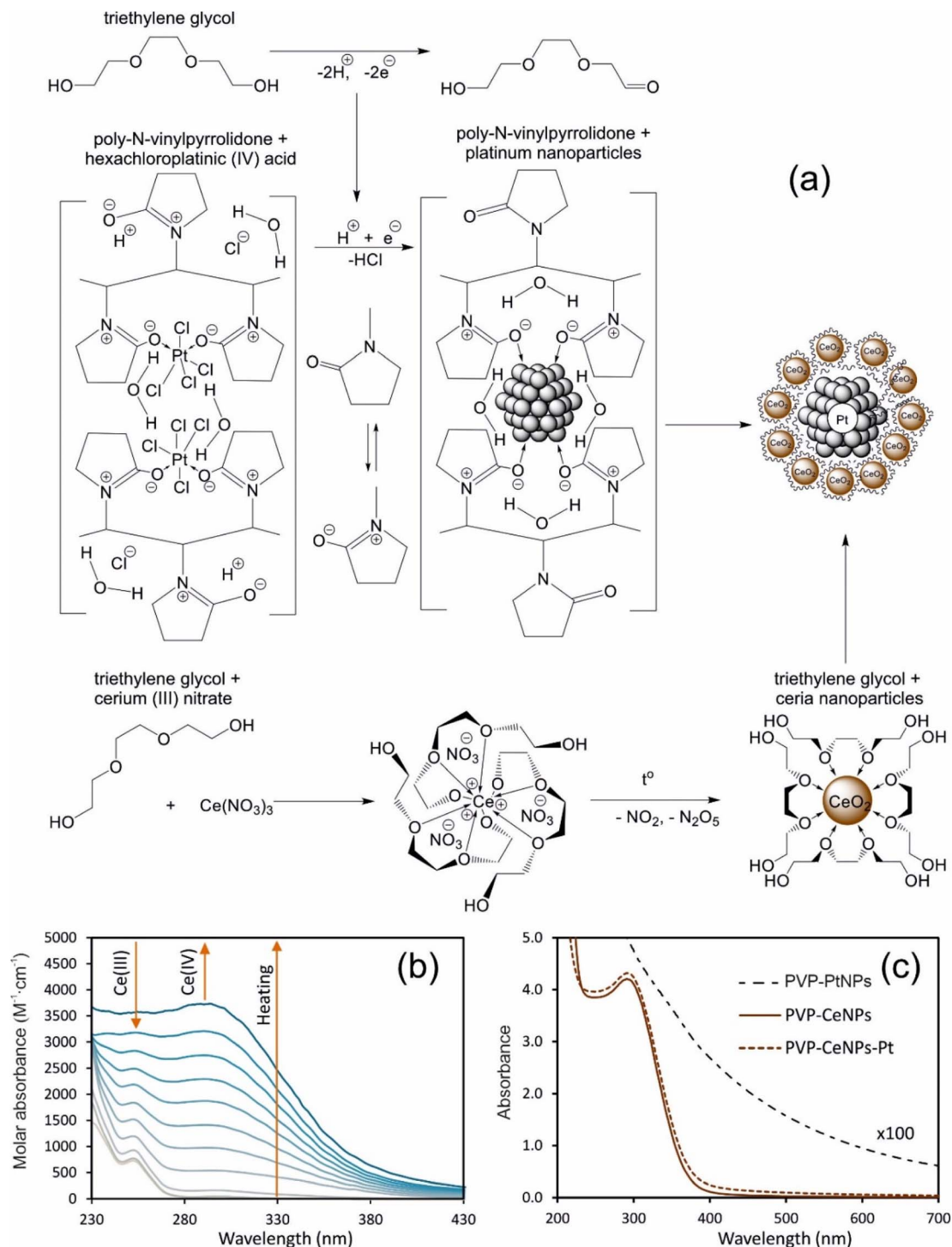
Fig. 1 (a) Schematic view of PVP–CeNPs–Pt nanocomposite synthesis by the high-temperature TEG process. (b) Dynamics of cerium species changes in the absorption spectrum of cerium(III) nitrate TEG solution in the absence of PVP during heating. (c) UV-vis absorption spectra of PVP-CeNPs, PVP-CeNPs–Pt (2 wt% Pt), and PVP-PtNPs. The concentration of NPs was the same for all samples.

relative concentration of $Pt^{\delta+}$ for the PVP-CeNPs–Pt compared to the PVP-PtNPs.

Thus, the proposed synthesis method by the decomposition of cerium nitrate in high-boiling glycol allows the synthesis of CeNP systems with a sufficiently high content of trivalent cerium cations in their composition, both in the presence and absence of platinum.

Chemical testing of the pro- and antioxidant activity of PVP-CeNPs, PVP-PtNPs, and PVP-CeNPs–Pt

Fenton-like activity. To date, the common view that CeNPs inactivate hydroxyl radicals ($^{\bullet}$OH) in living organisms is based on the observation that CeNPs inhibit dye discoloration in the Fenton reaction, as documented by Xue *et al.* in Tris–HCl buffer

Fig. 2 (Top) TEM micrograph of (a) PVP-CeNPs, (b) PVP-PtNPs, and (c) PVP-CeNPs–Pt nanocomposites. (Bottom) The Pt 4f, Ce 3d, and O 1s core level photoelectron spectra for all samples.
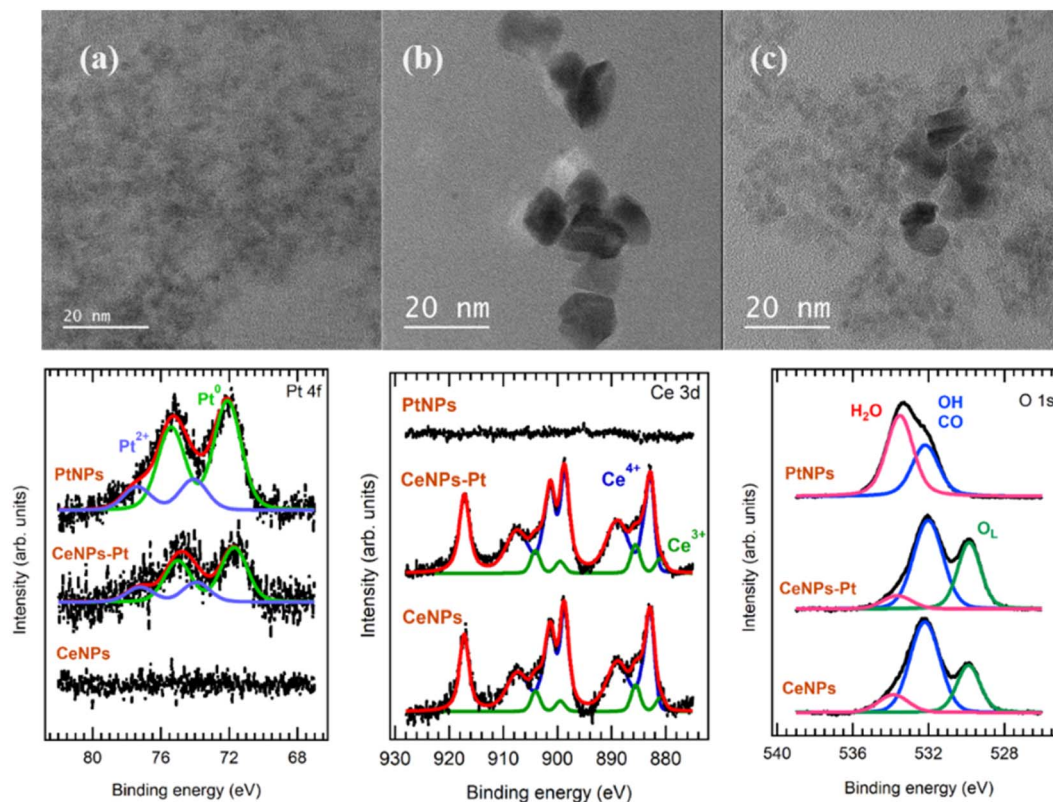
Table 1 The relative concentration of different Ce and Pt species for all NP systems

Samples	XPS				
	Ce^{3+}	Ce^{4+}	Ce^{3+}/Ce^{4+}	Pt^0	$Pt^{\delta+}$
PVP-CeNPs	10%	90%	0.11	—	—
PVP-PtNPs	—	—	—	78%	22%
PVP-CeNPs–Pt	11%	89%	0.12	73%	27%

at pH 4.7,[28] but this model does not seem entirely adequate. First, biological (cellular) systems typically do not have a pH as low as 4.7, and the extrapolation mentioned in that work is incorrect. Second, at such a low pH, tetravalent cerium species can oxidize hydrogen peroxide, and the decomposition of H_2O_2 can reduce the yield of ˙OH and distort the experimental results. Therefore, it is preferable to use systems in which the Fenton reaction proceeds under conditions of neutral pH values, while preventing hydrolysis of the iron salt. Such a Fenton process must be carried out with stable iron complexes, such as ethyl-enediamine tetraacetate (EDTA). According to Hu *et al.*, the EDTA-Fe^{3+} complex can increase the solubility of Fe^{3+} in a neutral environment and reduce the redox potential of Fe^{2+}/Fe^{3+}, thereby increasing the radical chain activity of Fe^{3+} and promoting the formation of intermediates, including hydroxyl (˙OH) and hydroperoxyl (HOO˙) radicals;[29] the superoxide anion

is also formed directly from dissolved oxygen (see Fig. S2, ESI†). Thus, in the EDTA-Fe^{3+}/H_2O_2 model, all the main ROS generated in biological systems are present at neutral pH values. All of the expected ROS, *i.e.* hydrogen peroxide (H_2O_2), superoxide anion $O_2^{˙-}$ and hydroxyl radical (˙OH), are capable of oxidative degradation of organic dyes, such as MB. The degradation of MB is accompanied by a color change, which was monitored spectrophotometrically. The concentration of the dye is proportional to its optical density at 662 nm (see Fig. S2, ESI†). The highest rate of MB discoloration by EDTA-Fe^{3+}/H_2O_2 was observed at pH 7.0.[30]

The kinetic curves of MB discoloration in the Fenton-like process at pH 7.0 are shown in Fig. 3(a1–a3); they follow the pseudo-first order reaction law and can be linearized in loga-rithmic coordinates as $\ln\left(\frac{[C_t]}{[C_0]}\right) = -kt$; where C_t and C_0 are the current and initial MB molar concentrations, t (min) is the reaction time, and $k\,(\mathrm{min}^{-1})$ is the reaction rate constant. Thus, the slope of the lines corresponds to the reaction rate constant k. The MB dye absorption obeys the Beer–Lambert law, $C_t \propto A_t$ $\Rightarrow \ln\left(\frac{[A_t]}{[A_0]}\right) = -kt$, where A_t and A_0 are the current and initial MB absorption. In this way, the reaction rate constants allow a quantitative comparison of the processes occurring in the systems (Fig. 3(a4)).

It is evident that CeNP sols enhance the rate of dye degradation under Fenton-like process conditions, with
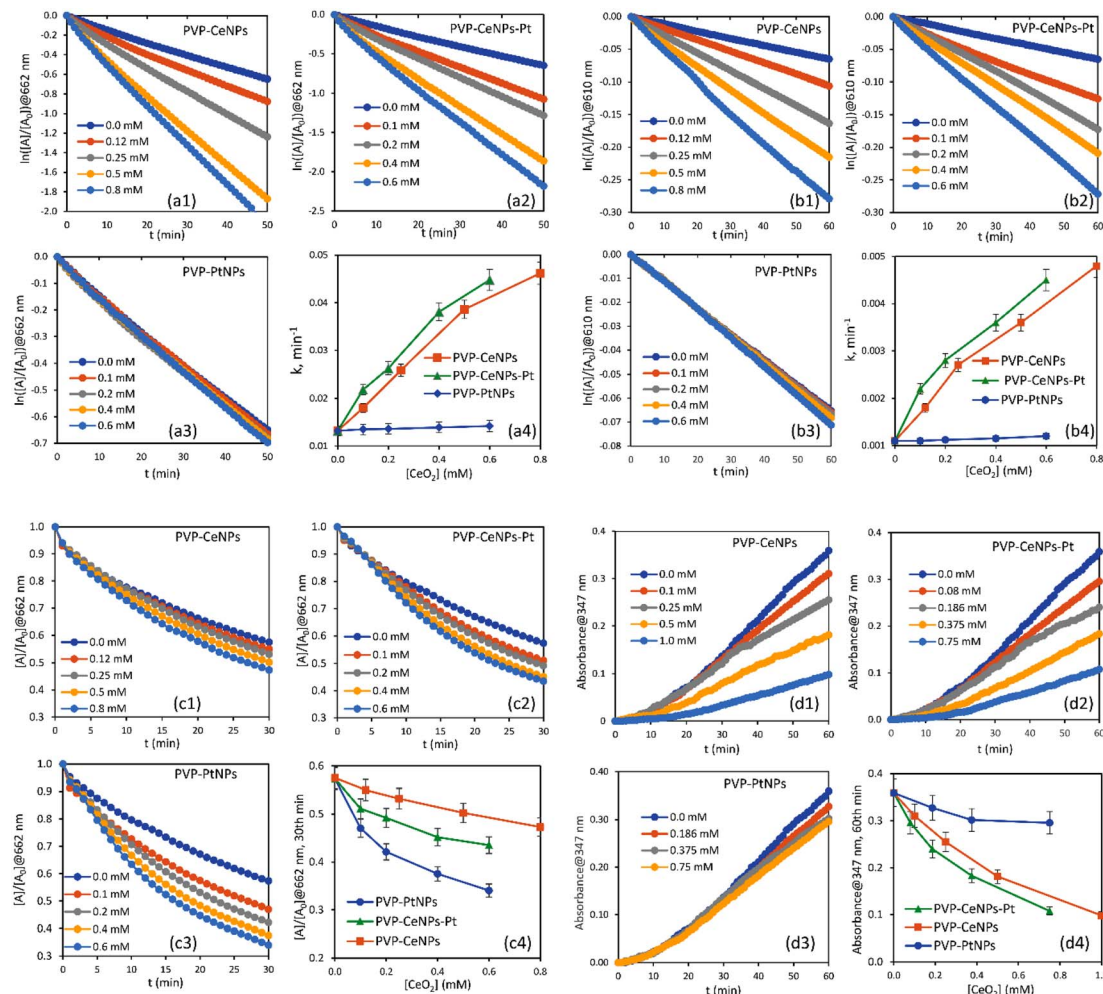
Fig. 3 (a1–a4) Kinetics of MB decomposition by Fenton's reaction at pH 7.0. (b1–b4) Kinetics of IC decomposition by hydrogen peroxide at pH 7.0. (c1–c4) Dynamics of MB bleaching by hypochlorite at pH 7.0. (d1–d4) Dynamics of adrenaline autooxidation at pH 10.5. (a1, b1, c1 and d1) PVP-CeNPs, (a2, b2, c2 and d2) PVP-CeNPs–Pt, (a3, b3, c3 and d3) PVP-PtNPs, (a4, b4, c4 and d4) summarized data. The concentration of NPs in mM units for each experiment is given in the legend or on the abscissa of the corresponding figure. The concentration of PVP-PtNPs is the same as for PVP-CeNPs–Pt nanocomposites, but without CeNPs.

a concentration-dependent effect (Fig. 3(a1)). The PtNPs, at the concentrations used in this study, had no discernible impact on the observed process (Fig. 3(a)). On the other hand, the presence of platinum in the PVP-CeNPs–Pt nanocomposite resulted in a slight increase in the pro-oxidant activity (Fig. 3(a2)). Interestingly, the published work of Yu et al. demonstrated that bovine serum albumin-stabilized PtNPs decompose Morin dye via a Fenton-like mechanism, with the oxidation process described by pseudo-first-order reaction kinetics.[31] As mentioned above, CeNPs are believed to provide protection against hydroxyl radicals.[28] Conversely, numerous studies have demonstrated the pro-oxidant effects of CeNPs in Fenton-like reactions, where organic dyes are decomposed. These studies have used a range of pH conditions, including acidic media at pH 3.0,[32] weakly acidic media at pH 5.8,[33] and neutral media at pH 7.0.[34] A study by Jain et al. investigated the effectiveness of a CeO$_2$-based Fenton reaction for the oxidative removal of MB dye. The results indicated that the most effective process occurs in neutral media in the pH range of 6.0–8.0.[35]

The CeNPs, prepared according to the scheme used in this work, contain a relatively high Ce^{3+} fraction. We suggest that the pro-oxidant activity of the PVP-CeNPs and PVP-CeNPs–Pt systems is due to the presence of Ce^{3+} cations in their composition. This conclusion is supported by the previous findings that the use of CeNPs enriched with trivalent cerium cations increases the probability of the peroxide-mediated process occurring via the Fenton pathway.[5]

Peroxidase-like activity. To evaluate whether PVP-CeNPs or PVP-CeNPs–Pt nanocomposites enhance the oxidative activity of the hydroxyl radical or exhibit peroxidase-like properties with H$_2$O$_2$ in the Fenton system, we studied the effect of NPs on the rate of dye decomposition under the influence of hydrogen peroxide alone, in the absence of the EDTA-Fe^{3+} complex. It should be noted that MB is slowly discolored by pure hydrogen peroxide solutions. Therefore, to facilitate the monitoring of oxidative degradation, a more readily oxidizable dye, indigo carmine (IC), was used in these studies. The discoloration of IC can be monitored spectrophotometrically, and the dye

concentration was determined by its optical density at 610 nm (see Fig. S3, ESI†).

The kinetic curves of IC dye decomposition by H_2O_2 also follow the pseudo-first order reaction law. The reaction rate constants allow a quantitative comparison of the processes occurring in the system (Fig. 3(b4)). It is evident that both PVP-CeNPs (Fig. 3(b1)) and PVP-CeNPs–Pt (Fig. 3(b2)) enhance the rate of hydrogen peroxide-induced discoloration of IC dye in a concentration-dependent manner. PtNPs, at the concentrations used, exert minimal influence on this process (Fig. 3(b3)), whereas their combination with the CeNP system slightly increases the pro-oxidant (peroxidase-mimetic) activity (Fig. 3(b4)).

In the analysis of the effect of CeNPs on IC bleaching by H_2O_2, it was reported that cerium oxide does not provide protection against hydrogen peroxide oxidation at acidic pH and exhibits peroxidase-like activity at pH 7.0,[4] the same as in the present study. Apoferritin-encapsulated PtNPs showed an increase in catalase activity with increasing pH and temperature. Conversely, peroxidase-like activity was observed to be optimal at physiological temperature and under slightly acidic conditions.[14]

Although MB is a more oxidatively stable dye than IC, the rate constant of the dye decomposition reaction by systems with CeNPs is an order of magnitude higher in the presence of iron ions. It can be concluded that the synthesized PVP-CeNPs and PVP-CeNPs–Pt nanocomposites will be active in biological systems in reactions of iron-dependent cell apoptosis (ferroptosis, see below), a process associated with iron dysregulation and oxidative stress by the Fenton reaction mechanism.

Hypochlorite bleaching activity. Hypochlorite ion (ClO^-) or hypochlorous acid (HClO) is one of the most important ROS with a key role in living systems. It is formed primarily in leukocytes as a result of the reaction between hydrogen peroxide and chloride ions in the presence of the enzyme myeloperoxidase.[36] Hypochlorite plays an active role in the antibacterial defense of the body, killing pathogens during infections. However, excess ClO^- damages biological tissues and causes oxidative stress-related dysfunction. The toxic amount of HClO is less than that of H_2O_2, because cells lack an enzymatic scavenging system for HClO.[37] Hypochlorite readily bleaches a variety of dyes by the formation of active oxygen: $ClO^- \leftrightarrow Cl^- + [O]$. We have used the MB dye to study this process (see Fig. S4 (a), ESI†).

Hypochlorous acid has two distinct absorption peaks at 237 nm with a molar absorption coefficient (ε) of 102 M^{-1} cm^{-1} and at 289 nm with $\varepsilon = 36.1$ M^{-1} cm^{-1}. The absorption peak of ClO^- occurs at 292 nm with $\varepsilon = 378$ M^{-1} cm^{-1}.[38] At physiological pH 7.0, hypochlorite predominantly exists in the nonionic (acidic) form. The PVP-CeNPs and PVP-CeNPs–Pt have an adsorption band at 290 nm with a molar absorption coefficient of approximately 4000 M^{-1} cm^{-1}. Thus, the behavior of these systems in the presence of hypochlorite can be studied as shown in Fig. S4(b–d) of the ESI.† All NP systems demonstrated the ability to accelerate the decomposition of HClO to varying degrees. The maximum rate of optical density decrease at the

characteristic wavelength of 292 nm was observed for PVP-CeNPs–Pt (see Fig. S4(c), ESI†).

The dynamics of the MB dye discoloration is shown in Fig. 3(c1, c2 and c3). In order to compare the influence of the studied NPs on this process, the relative decrease of the optical density of the dye at 662 nm at the 30th minute of the experiment was evaluated. As shown in Fig. 3(c4), all systems facilitate the degradation of the MB dye by hypochlorite, with PVP-PtNPs showing the highest values and PVP-CeNPs the lowest. An intermediate value was obtained for the PVP-CeNPs–Pt nanocomposite, indicating that platinum enhances the pro-oxidant properties of cerium oxide against hypochlorite in the MB dye discoloration process.

Superoxide dismutase-like activity. Another important ROS generated in biological systems is the superoxide anion radical ($O_2^{\cdot-}$). The next step of this research was to study how PVP-CeNPs and PVP-CeNPs–Pt nanocomposites influence its behavior and dismutation within the system. In other words, the question is whether the synthesized NP systems can mimic superoxide dismutase (SOD) activity. It is known that the SOD-like activity of CeNPs can be measured by inhibiting the autoxidation of adrenaline (AD),[39] since the process proceeds through the intermediate formation of superoxide (Fig. S5, ESI†).

The kinetic curves in Fig. 3 (d1, d2 and d3) show that all of the studied systems exhibited SOD-like activity and effectively inhibited the autoxidation of AD. For a more comprehensive interpretation of the results related to the different solutes, the optical density data at 347 nm (indicating the amount of oxidation product generated by AD) at 60 min from the start of the experiment were compared in Fig. 3(d4). All investigated systems demonstrate a concentration-dependent reduction in the formation of the AD oxidation products. In particular, PVP-PtNPs show minimal activity with platinum concentrations, fifty times lower than those reported for PVP-CeNPs. At the same time, the incorporation of Pt (2 wt%) was observed to enhance the SOD-like activity of PVP-CeNPs. Klochkov et al. used this methodology to investigate the SOD mimetic activity of citrate-stabilized CeNPs and demonstrated that an increase in CeNPs concentration within a certain range resulted in a reduction in SOD activity, which was attributed to an increase in NPs agglomeration.[40] This phenomenon was not observed in our study, possibly due to the enhanced stabilizing capacity of PVP in an alkaline environment.

Biological *in vitro* testing of PVP-CeNPs, PVP-PtNPs, and PVP-CeNPs–Pt

Toxicity. The analysis of metabolic activity (MTT assay) and total live adherent cell number (CV staining of adherent cells) showed that the synthesized NPs exhibited low toxicity at concentrations of up to 1 mM PVP-CeNPs (Fig. 4). This finding provides indirect evidence for the low toxicity of the system components. In fact, polyvinylpyrrolidone (PVP) K-17 is used in medical applications, and TEG is recognized as having a very low acute toxicity *via* intravenous, intraperitoneal, oral, dermal, and inhalation routes of administration.[41] The PtNPs were found to be non-toxic within the concentration range used.
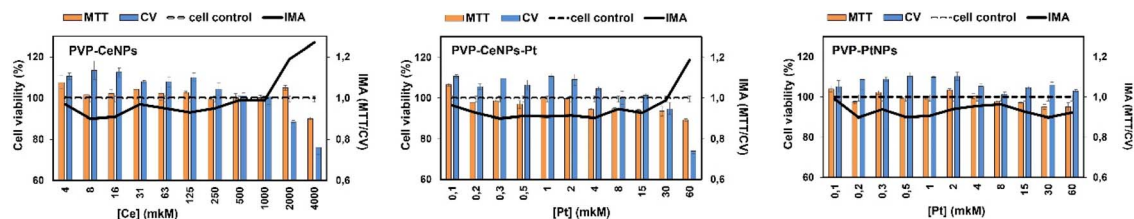
Fig. 4 Metabolic activity (MTT), viability (CV), and the index of metabolic activity (IMA) of MA-104 cells in the presence of PVP-CeNPs, PVP-CeNPs–Pt, and PVP-PtNP sols prepared by double dilution with water.

However, Pt inclusion in PVP-CeNPs exhibited a slight increase in the cytotoxicity and a corresponding decrease in the index of metabolic activity (IMA), defined as the ratio of metabolic activity to the total number of adherent living cells. Both PVP-CeNPs and PVP-CeNPs–Pt showed a decrease in IMA at low concentrations and an increase at high concentrations. The comparison between these two systems allows us to conclude that the presence of Pt in the PVP-CeNPs–Pt nanocomposite has an inhibitory effect on the IMA values (Fig. 4).

In vitro toxicity assessment uses a set of criteria to quantitatively evaluate the response of the cell culture to the effects of varying concentrations of NP systems. Toxicity is determined by the inhibitory concentration criterion, which reflects the varying percentage of cell destruction or function inhibition. Since the synthesized NP systems did not cause a reduction in the metabolic activity or destruction of the cell monolayer to an extent equal to or higher than 50%, an indicator, IC_0, was calculated (Table 2), which represents the maximum concentration of NPs that does not induce changes in metabolic activity of the total number of adherent cells, as determined by the methods used, compared to the control MA-104 cells. Based on the data presented in Table 2, it can be concluded that the criterion limiting the toxicity of PVP-CeNPs is the metabolic activity of the cells (MTT assay). For PVP-PtNPs, the critical indicator is the inhibition of the total number of adherent cells (CV assay). Thus, cells respond differently to PVP-CeNPs and PVP-PtNPs. In particular, the IC_0 values in the MTT and CV assays differ by a factor of 2 for PVP-CeNPs and by a factor of 10 for PVP-PtNPs (Table 2, IC_0 ratio MTT/CV). The cytotoxic properties of PVP-CeNPs–Pt are 1.5–2 times higher than those of PVP-CeNPs and PVP-PtNPs in the CV assay and by 2–20 times higher in the MTT assay. The presence of Pt in the PVP-CeNPs–Pt reduces the IC_0 ratio MTT/CV by more than 10 times compared to PVP-CeNPs to a level close to that of PVP-PtNPs.

Table 2 Non-toxic (IC_0) concentrations of PVP-CeNPs, PVP-CeNPs–Pt, and PVP-PtNP nanocomposites

Samples	IC_0 (MTT assay)		IC_0 (CV assay)		IC_0 ratio MTT/CV	
	Ce, μM	Pt, μM	Ce, μM	Pt, μM	Ce	Pt
PVP-CeNPs	3684	—	1839	—	2.00	—
PVP-CeNPs–Pt	178	71	1266	506	0.14	0.14
PVP-PtNPs	—	123	—	≥1200	—	0.10

The observed decrease of IMA in the presence of PVP-PtNPs and PVP-CeNPs–Pt, caused by the inhibition of the metabolic activity of cells, correlates with the known data on the inhibition of the mitochondrial metabolism in tumor cells by platinum compounds[42] and is one of the determining factors for the implementation of their antitumor action. Our results show that this effect is also present to some extent in monkey kidney cells MA-104.

Pro- and antioxidant activities. The effects of the studied NP systems on the oxidative stress developed in MA-104 cells are shown in Fig. 5. To evaluate the impact of Pt on the pro- or antioxidant properties of PVP-CeNPs, the results are presented in μM units of platinum concentration in PVP-CeNPs–Pt (Fig. 5(a2, a5, b2 and b5)) and PtNPs (Fig. 5(a3, a6, b3 and b6)). The concentration of CeNPs in PVP-CeNPs–Pt is identical to that in PVP-CeNPs.

Fig. 5(a1–a3) show that all synthesized systems increased H_2O_2-induced oxidative stress when administered to cells in a prophylactic regimen, and the presence of Pt enhanced the pro-oxidant activity of PVP-CeNPs. This is evidenced by a decrease in the viability index (Fig. 5(a2)). The *in vitro* data corroborate the results of the chemical tests presented above, indicating that all NPs exhibit peroxidase-like activity towards organic molecules (dyes) and biological objects (cells). At the same time, PVP-PtNPs, which have minimal peroxidase activity in chemical tests, markedly enhance the toxicity of H_2O_2 in MA-104 cell culture under a preventive treatment regimen (Fig. 5(a3)). In the therapeutic regimen (after addition of H_2O_2, as shown in Fig. 5(a4–a6)), the pro-oxidant effect of all systems was significantly lower than in the prophylactic regimen. However, as observed in the prophylactic regimen, the presence of Pt in the PVP-CeNPs–Pt nanocomposite reduced the integral indicator, or viability index (Fig. 5(a5)).

Ferroptosis. An iron-related type of programmed cell death is referred to as ferroptosis, which is characterized by an increase in ROS based on the Fenton reaction.[43] Lewerenz *et al.* proposed that oxytosis and ferroptosis should be considered as two names for the same cell death pathway. It was concluded that the molecular pathways of ferroptosis and oxytosis are very similar, if not identical.[44] Therefore, it is reasonable to expect a similarity in the pro-oxidant behavior of NPs in both cases. The induction of ferroptosis is due to the inhibition of cysteine uptake or the inactivation of glutathione peroxidase 4 (GPX4). Consequently, cystine/glutamate regulators and GPX4 inhibitors, such as erastin or sulfasalazine (SAS), are considered as traditional inducers of ferroptosis.[45]
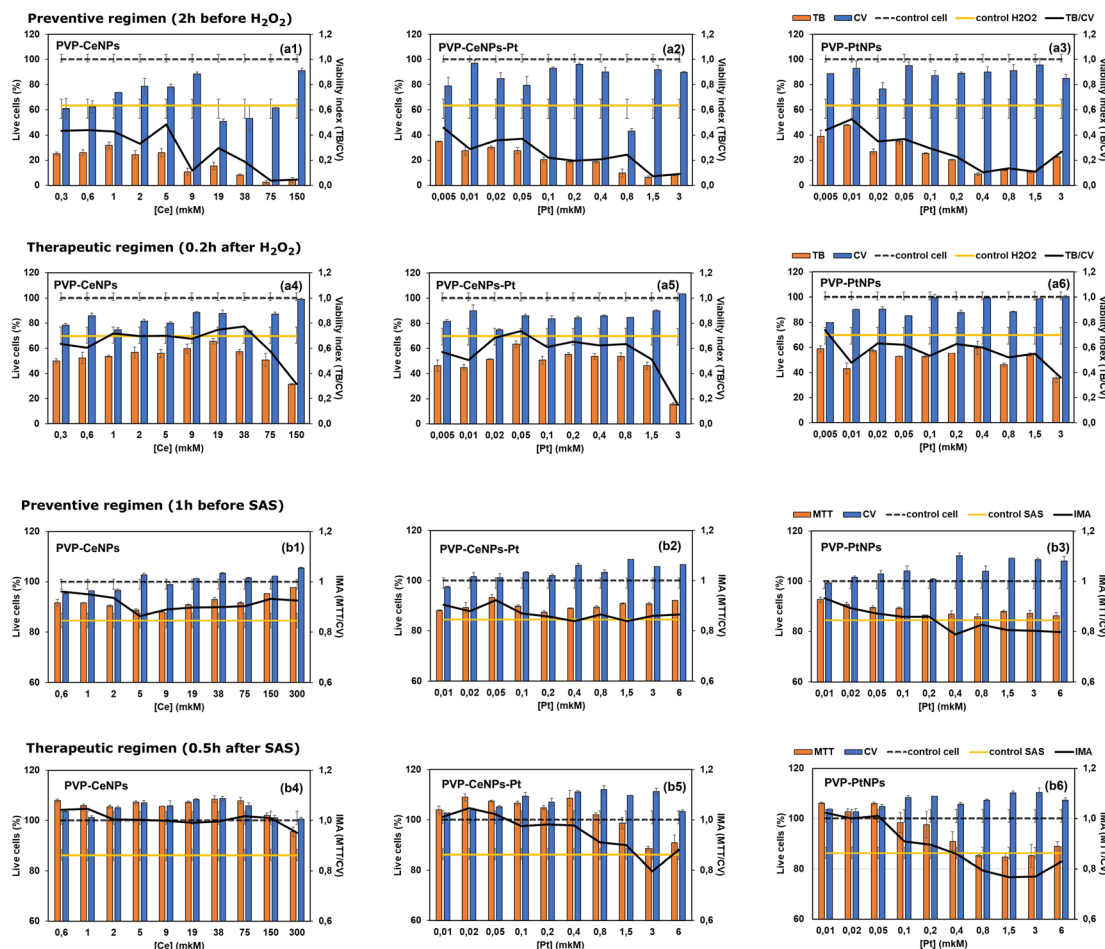
Fig. 5 (a, orange) Viability in TB exclusion assay, (b, orange) metabolic activity in MTT assay, (a, b, blue) viability of adherent cells in CV assay, and (a, black) index of viability (TB/CV) and (b, black) index of metabolic activity (IMA) of MA-104 cells in the presence of different concentrations of PVP-CeNPs, PVP-CeNPs–Pt, and PVP-PtNP sols under the condition of: (a) oxytosis caused by H₂O₂ during (a1, a2 and a3) prophylactic and (a4, a5 and a6) therapeutic regimens; (b) ferroptosis caused by sulfasalazine (SAS) during (b1, b2 and b3) preventive and (b4, b5, b6) therapeutic regimens. The concentration of CeNPs in PVP-CeNPs–Pt is identical to that in PVP-CeNPs.

In the event of failure of the iron homeostasis mechanisms and the emergence of Fenton-like processes, it is expected that PVP-CeNPs or PVP-CeNPs–Pt will facilitate programmed cell death *in vitro*, as they have been shown to stimulate the Fenton-like process in the chemical tests presented above. However, the effect of NPs in the case of ferroptosis is significantly different. When administered prophylactically, they have little effect on the metabolic activity of the cells (Fig. 5(b1–b3)). In contrast, when administered after the onset of ferroptosis, they almost completely restore the IMA of the cells (therapeutic regimen, see Fig. 5(b4–b6)). The presence of Pt in PVP-CeNPs–Pt was observed to slightly reduce the protective ability of PVP-CeNPs, thereby enhancing the pro-oxidant effect. A comparison of PVP-PtNPs and PVP-CeNPs–Pt (Fig. 5(b6 and b5)) shows that the latter system enhances metabolic activity over most of the concentration range. The data indicate that PVP-CeNPs and PVP-CeNPs–Pt protect cells against SAS-induced ferroptosis to varying degrees. This suggests the presence of an additional mechanism by which NPs affect ferroptosis in cells, distinct from the peroxidase-like activity and enhancement of the

Fenton-like reaction. Zhang *et al.* showed that CeNPs significantly restored the expression of GPX4 and mitochondrial-associated proteins, thereby inhibiting ferroptosis.[46] The present results suggest that PVP-CeNPs and PVP-CeNPs–Pt may serve as promising candidates for the prevention and treatment of ferroptosis in cardiomyocytes. It can be concluded that the studied NP systems, when administered therapeutically, do not participate in oxidative stress as oxidoreductase mimetics, but rather reduce the toxic (initiating) effect of the ferroptosis inducer (SAS) in this process.

Materials and methods

Synthesis of NP systems

Materials. Cerium(III) nitrate hexahydrate (Ce(NO₃)₃·6H₂O), poly-*N*-vinylpyrrolidone (PVP, K17), triethylene glycol (TEG), methylene blue (MB) dye, indigo carmine (IC) dye and adrenaline (AD) were purchased from Sigma-Aldrich. Hexachloroplatinic(IV) acid hexahydrate (H₂PtCl₆·6H₂O) (99.9% purity) in hydrochloric acid solution (~40% of Pt), hydrogen

peroxide (H₂O₂), and sodium hypochlorite (NaClO) were purchased from Reachim and used as received.

Synthesis. PVP-stabilized CeNPs (PVP-CeNPs) were synthesized by the following method: a solution of Ce(NO₃)₃·6H₂O (2.17 g, 5 mmol) and PVP (0.4 g) in water (2 ml) was prepared and then mixed with TEG (50 ml). The solution was heated at 250 °C with intensive stirring for about 3 h. During this time, the solution gradually changed its appearance, becoming cloudy, white, yellow, brown opaque, and finally dark brown and transparent. The heating was continued until any trace of the suspended phase had disappeared and the formation of brownish nitrogen oxide fumes ceased (Fig. S1, ESI†). During the thermal treatment, the disproportionation of cerium(III) nitrate occurred, resulting in the formation of cerium(IV) and nitrogen oxides: $Ce(NO_3)_3 \rightarrow CeO_2\downarrow + NO_2\uparrow + N_2O_5\uparrow$ (Fig. 1). The solution was then cooled to room temperature and dialyzed against distilled water for 240 h with magnetic stirring. The retentate was diluted with distilled water (200 ml) and the system was sonicated for approximately 30 min to obtain a yellowish transparent opalescent sol.

PVP-stabilized Pt–CeNP nanocomposites (PVP-CeNPs–Pt) were synthesized by a one-pot stepwise method starting with the high-temperature glycol reduction of Pt^{4+} as follows: the Pt precursor (corresponding to 2% of Pt in the nanocomposite or 20 mg of Pt) and PVP (400 mg) were dissolved in water (2 ml) and then mixed with TEG (50 ml). The solution was then heated to 200 °C with continuous stirring for about 3 h. The color of the solution changed from golden yellow to brown and then to almost black (transparent in a thin layer), indicating the formation of PVP-PtNPs (Fig. S1, ESI†). The glycol sol was then cooled to room temperature, and a cerium(III) nitrate solution was added to the system, allowing the synthesis of PVP-CeNPs to proceed as previously described. A schematic representation of the synthesis of the PVP-CeNPs–Pt nanocomposite is shown in Fig. 1(a). The retentate was then processed as described above, resulting in a gray-brownish transparent opalescent sol. All systems were analyzed for NPs content and stored in the dark prior to use.

Characterization of NP systems

UV-vis spectrophotometry. UV-vis (200–700 nm) characterization of the nanocomposites and spectrophotometric experiments were performed using a P2 single beam UV/VIS spectrophotometer (Shanghai Mapada Instruments Co. Ltd).

Transmission electron microscopy. The NP systems were characterized by high resolution TEM (JEOL JEM-2200FS microscope, the point resolution is 0.2 nm with lattice resolution of 0.1 nm) using an accelerating voltage of 200 kV. Original sols (PVP-CeNPs, PVP-PtNPs, and PVP-CeNPs–Pt) were ultrasonicated for 10 min and mixed with ultrapure water in a ratio of 1 : 50 or 1 : 100 (depending on the optical density of the NP sols). A drop of the mixture was then placed on a carbon-coated copper grid and left to dry in the air. The grain diameter of 200 to 400 NPs was measured for each sample. The post-processing of the acquired images was done using ImageJ software.

X-ray photoelectron spectroscopy. For the XPS analysis, the colloidal solution of NPs was ultrasonicated for 25 min. 10 μl of PVP-CeNPs, PVP-PtNPs, and PVP-CeNPs–Pt were placed on an unpolished glassy carbon substrate previously cleaned by Ar ion sputtering (60 min, 1 kV) and then the samples were dried in a desiccator. The time to obtain the dry spot on the glassy carbon was 60 min for PVP-PtNPs and 5 min for PVP-CeNPs and PVP-CeNPs–Pt systems. The glassy carbon plate was attached to a holder with carbon tape and inserted in the ultra-high vacuum chamber of the photoelectron spectrometer. A laboratory Al Kα radiation source was used for the acquisition of the Pt 4f, Ce 3d, and O 1s core level spectra with a total resolution of about 1 eV.

Chemical testing of the pro- and antioxidant activity of NP systems

Fenton-like process and activity. A freshly prepared solution of FeCl₃ (2 mM), EDTA (3 mM), and MB (20 μM) was adjusted to a hydrogen potential value of pH 7.0. Then, 1.0 ml of 5% hydrogen peroxide was rapidly injected into 50 ml of this solution, stirred, and the discoloration of the dye was kinetically monitored using a spectrophotometer at a wavelength of 662 nm (Fig. S2, ESI†). Selected amounts of NPs were then introduced into the system to investigate their pro- or antioxidant activity. This was achieved by adding 0.1–1.0 ml of 0.04 M PVP-CeNPs or 0.03 M PVP-CeNPs–Pt sols followed by the selected amount of hydrogen peroxide. The concentration of platinum in the PVP-PtNP experiments is equivalent to that in the PVP-CeNPs–Pt experiments, but without cerium oxide. The pH was monitored before and after the experiments, and the value remained stable, with a variation of ±0.01. This ensured that any buffer affecting the results could be excluded.

Peroxidase-like activity. All experimental conditions were identical to those described in the previous paragraph except for the iron complex. Indigo carmine dye (IC) was used instead of MB. The kinetics of IC degradation were recorded at a wavelength corresponding to the absorption band maximum of 610 nm (Fig. S3, ESI†).

Hypochlorite bleaching activity. The pH of the MB solution (20 μM) was adjusted to a value of 7.00 ± 0.02 by adding 0.5 ml of sodium hypochlorite (1% active chlorine) to 50 ml of the dye solution. After injection of sodium hypochlorite, the solution was stirred rapidly, and the kinetics of dye staining was examined using the spectrophotometer at a wavelength of 662 nm (Fig. S4, ESI†). Appropriate amounts of NPs were then introduced into the system by adding 0.1–1.0 ml of 0.04 M PVP-CeNPs or 0.03 M PVP-CeNPs–Pt sols prior to the addition of hypochlorite. The platinum concentration in the PVP-PtNP experiments is the same as in the PVP-CeNPs–Pt experiments, but without the inclusion of ceria. The pH was kept at a constant level and monitored before and after the experiments, with a maximum variation of ±0.02. This ensured that any potential buffer effects on the results could be excluded.

Superoxide dismutase-like activity. The experimental protocol was essentially identical to that described in the previous article.[39] In summary, the PVP-CeNPs, PVP-PtNPs, and PVP-CeNPs–Pt sols were prepared at an appropriate concentration (0.08–1.00 mM CeO₂) and adjusted to pH 10.5 using a NaOH solution. The concentration of Pt in PVP-PtNPs is

equivalent to that of the PVP-CeNPs–Pt nanocomposites and is expressed in units of cerium concentration for comparison. To 2 ml of the prepared solution, 0.1 ml of 0.18% adrenaline (AD) was rapidly injected and then stirred. The solution was then placed in a spectrophotometer cell, and the absorbance was recorded at 347 nm for 60 min in 1 min increments (Fig. S5, ESI†). The reference solutions used for baseline calibration contained all components except AD.

Biological testing of toxicity, pro- and antioxidant activity of NP systems

Cell cultures. Embryonic kidney cells of the African green monkey (*Cercopithecus aethiops*, MA104 cell line, ATCC® CRL-2378.1™) were provided by GlaxoSmithKline and stored in the cell culture collection of the Zabolotny Institute of Microbiology and Virology, Ukraine. To form a cell monolayer, 0.1 ml of a suspension containing 3×10^5 cells per ml was added to the wells (96-well plates, Costar) and incubated for 24 h at 37 °C in a TC-80 M-2 thermostat (98% humidity, 5% CO_2). The growth medium used was synthetic nutrient medium DMEM/F12 (Sigma, USA), containing 8% fetal calf serum (Sigma, USA), 25 mM HEPES, 10 mM glutamine, and an antibiotic-antimycotic solution (Biowest). After 24 h of cultivation, the state of the monolayer of cells in the plates was monitored using an inverted light microscope. Plates with a confluent monolayer of cells were used for the study. The maintenance medium consisted of DMEM/F12 medium, 2% fetal calf serum, 25 mM HEPES, and 10 mM glutamine. DMEM/F12 medium was used to wash the cell monolayer. The NP samples were suspended in distilled water by serial doubling dilution, transferred to the maintenance medium in the wells of a 96-well plate (100 µl) with confluent cell monolayer in a ratio of 1/10 (v/v), and kept together for 24 h at 37 °C in humid air (98%) containing 5% CO_2. The cellular uptake of NPs was then monitored using Trypan blue, Crystal violet, and MTT assays. Each assay allows us to determine a different aspect of the cellular response. The combined use of multiple assays and the calculation of the corresponding indices based on the data obtained allows for a more holistic view of the cellular response to the interaction with NPs. Each experiment was repeated three times with four replicates.

Trypan blue (TB) exclusion assay. The dye exclusion test is used to determine the number of viable cells present in a cell suspension/monolayer. It is based on the principle that living cells have intact cell membranes that exclude TB.[47] Briefly, cells were exposed to the tested sols of different concentrations (0.1–5.0 mM) as described above, and at the end of the exposure period, the culture medium was removed from the wells of the 96-well plates, and 0.2% TB solution in PBS (100 µl per well) was added. After 3–5 min, the dye solution was removed, and the cells were washed twice with PBS to remove any remaining dye. The absorbance of the wells was read spectrophotometrically at 540 nm in a Thermo/LabSystems Multiskan MS Microplate Reader. The percentage of viable cells in the experimental wells was calculated using the formula: $100 - (OD_{exp}/OD_{contr}) \times 100\%$, where OD_{exp} – optical density in experimental wells and OD_{cont} – optical density in control wells. In the study, intact

untreated cells were used as a control. This technique measures cell viability, but has the disadvantage that viability is indirectly determined by the integrity of the cell membrane.

Crystal violet (CV) assay. Cells were exposed to sols of different concentrations (0.1–5.0 mM). At the end of the exposure period, the culture medium was removed and 0.5% CV solution in 30% C_2H_5OH (100 µl per well) was added. The cells were stained for 10 min at room temperature. The dye was removed, and the cells were carefully washed with water to completely remove any excess of unbound dye, the plates were dried, and 0.1 ml 70% C_2H_5OH was added to the wells, *i.e.* to the stained adhesive cells to dissolve the dye. The plates were shaken for 5 min, placed in a Thermo/LabSystems Multiskan MS Microplate Reader, and the absorbance was then read spectrophotometrically at 540 nm. The percentage of adherent viable cells in the experimental wells was determined using the formula ($OD_{exp}/OD_{contr}) \times 100\%$, where OD_{exp} is the optical density in the experimental wells and OD_{cont} is the optical density in the control wells. In the study, intact untreated cells were used as a control.

The index of viable cells (TB/CV) was calculated using the formula C_{TB}/C_{CV}, where C_{TB} (%) is the calculated percentage of viable cells relative to control cells taken as 100%; C_{CV} (%) is the calculated percentage of adherent viable cells relative to control cells taken as 100%. Since the control cells are assigned a value of 100% in both the TB and CV assays, their metabolic activity index is therefore 1.

Metabolic assay (MTT). Cells were exposed to sols of different concentrations (0.1–5.0 mM). 2 h before the end of the exposure period, the culture medium was removed from the plates with confluent cell monolayer, and MTT solution (3-(4,5-dimethyl-2-thiazolyl)-2,5-diphenyl-2*H* tetrazolium bromide, Sigma-Aldrich) in PBS (0.1 mg ml^{-1}, 100 µl per well) was added to the cells. At the end of the exposure period, the supernatant liquid was removed, and a lysis solution containing 0.1% SDS (Sigma-Aldrich) solution in DMSO (Sigma-Aldrich) was added. The plates were shaken for 5 min and placed on a Thermo/LabSystems Multiskan MS Microplate Reader, and the absorbance was read colorimetrically at 492 nm. Each experiment was repeated three times with four replicates.

The index of metabolic activity (IMA) was calculated using the formula C_{MTT}/C_{CV}, where C_{MTT} (%) is the calculated percentage of metabolically active cells relative to control cells taken as 100%; C_{CV} (%) is the calculated percentage of adherent viable cells relative to control cells taken as 100%. Since the values of the control cells are taken as 100% in both the MTT and SV assays, their metabolic activity index is 1.

Pro- and antioxidant activity. The assay was performed as previously described[48] in therapeutic (0.2 h after treatment with H_2O_2) and prophylactic (2 h before treatment with H_2O_2) schemes. Briefly, the samples of NPs of different concentrations (60 µM–4.0 mM) were added to the confluent cell monolayer in a ratio of 1/10 (v/v) 30 min after or before the H_2O_2 treatment (the final concentration of H_2O_2 in each well was 0.5 mM), 2 h after the application of H_2O_2 the cell metabolic activity was determined by MTT assay, and the number of surviving cells was determined as previously described to define the total viability of the cells in the CV assay.

Ferroptosis-interference activity. Ferroptosis was induced by treating cells with sulfasalazine (SAS) (Fig. S6, ESI†). Briefly, an 80 mM stock solution of SAS in dimethyl sulfoxide (DMSO) (Sigma) was diluted to the 0.8 mM working concentration. A 1/100 (v/v) solution of SAS was then added to the culture medium in the wells where a monolayer of cells had formed. The assay was performed in therapeutic (0.5 h after SAS treatment) and prophylactic (1 h before SAS treatment) schemes. Cell viability was assessed after 24 h. Metabolic activity (MTT assay) and the total number of adherent viable cells (CV assay) were quantified, and IMA was calculated for each sample.

Conclusions

PVP-stabilized sols of cerium oxide, platinum, and their composition (PVP-CeNPs, PVP-PtNPs, and PVP-CeNPs–Pt) were prepared by a novel TEG-mediated procedure and used to study the oxidoreductase mimetic enzyme activity in the dye model chemical tests and in living cell culture. The PVP-CeNPs, whether in the presence or absence of Pt, contain a significant amount of Ce^{3+} and exhibit pro-oxidant activity in inanimate systems at a neutral value of pH 7.0. They facilitate dye discoloration in Fenton-like reaction models, act as peroxidase mimetics in the oxidation of dyes by hydrogen peroxide, and enhance hypochlorite bleaching. In addition, all NP systems inhibit the autoxidation of catecholamines (AD) processed via the superoxide pathway and act as SOD mimetics in a dose-dependent manner. The presence of Pt enhances the oxidoreductase-like activity of PVP-CeNPs in peroxidase, SOD-like, and Fenton-like processes.

In living cell culture, PVP-CeNPs and PVP-CeNPs–Pt possess pro-oxidant oxidoreductase-like activity and enhance hydrogen peroxide-induced oxytosis. However, they were found to abolish the ferroptosis metabolic activity induced by sulfasalazine. The synthesized NP systems exhibited low cytotoxicity (according to CV assay) and induced a slight decrease in the metabolic activity of cells (according to MTT assay), regardless of the Pt content in PVP CeNP sols. Overall, the biological tests of this study have provided a basis for understanding the interactions of PVP-CeNPs–Pt nanocomposites with cells, allowing their tailor-made synthesis for biomedical applications. In addition, the different responses of the NPs in the chemical tests confirm the complexity of real biological systems and the difficulty of simulating them in the laboratory.

Data availability

Data for this article, including microscopy, photoemission and *in vitro* dataset, are available at the Elettra Sincrotrone Trieste repository at **https://doi.org/10.34967/I41724**. The KolXPD software was used for the photoemission dataset. Also, the data supporting this article have been included as part of the ESI.†

Author contributions

N. M. Z.: conceptualization, investigation, methodology, supervision. I. V. D. and A. D.: data curation, formal analysis,

writing – original draft. V. K. and J. N.: data curation, formal analysis, investigation. I. M.: funding acquisition, methodology, writing – review & editing. K. C. P.: funding acquisition, writing – review & editing. T. S.: formal analysis, methodology, writing – review & editing. A. B. S.: conceptualization, investigation, methodology, writing – review & editing. N. T.: conceptualization, methodology, supervision, writing – review & editing.

Conflicts of interest

There are no conflicts to declare.

Acknowledgements

References

1 N. Singh, G. R. Sherin and G. Mugesh, *Angew. Chem., Int. Ed.*, 2023, **62**, e202301232.

2 C. Xu and X. Qu, *NPG Asia Mater.*, 2014, **6**, e9016.

3 S. Singh, *Biointerphases*, 2016, **11**, 04B202.

4 A. L. Popov, A. B. Shcherbakov, N. M. Zholobak, A. Y. Baranchikov and V. K. Ivanov, *Nanosyst.: Phys. Chem. Math.*, 2016, **8**, 760–781.

5 A. B. Shcherbakov, N. M. Zholobak and V. K. Ivanov, in *Metal Oxides: Properties and Applications*, ed. S. Scirè and L. Palmisano, Elsevier, 2020, pp. 279–358.

6 M. S. Lord, J. F. Berret, S. Singh, A. Vinu and A. S. Karakoti, *Small*, 2021, **17**, 2102342.

7 G. Pellavio, M. P. Demichelis, P. Sommi, U. Anselmi-Tamburini, C. Scotti and U. Laforenza, *Int. J. Mol. Sci.*, 2024, **25**, 372–388.

8 M. Moglianetti, E. De Luca, D. Pedone, R. Marotta, T. Catelani, B. Sartori, H. Amenitsch, S. F. Retta and P. P. Pompa, *Nanoscale*, 2016, **8**, 3739–3752.

9 H. Ye, Y. Liu, A. Chhabra, E. Lilla and X. Xia, *ChemNanoMat*, 2017, **3**, 33–38.

10 K. Hirakawa and S. Sano, *Bull. Chem. Soc. Jpn.*, 2009, **82**, 1299–1303.

11 A. Watanabe, M. Kajita, J. Kim, A. Kanayama, K. Takahashi, T. Mashino and Y. Miyamoto, *Nanotechnology*, 2009, **20**, 455105.

12 M. Kajita, K. Hikosaka, M. Iitsuka, A. Kanayama, N. Toshima and Y. Miyamoto, *Free Radical Res.*, 2007, **41**, 615–626.

13 T. Hamasaki, T. Kashiwagi, T. Imada, N. Nakamichi, S. Aramaki, K. Toh, S. Morisawa, H. Shimakoshi, Y. Hisaeda and S. Shirahata, *Langmuir*, 2008, **24**, 7354–7364.

14 J. Fan, J.-J. Yin, B. Ning, X. Wu, Y. Hu, M. Ferrari, G. J. Anderson, J. Wei, Y. Zhao and G. Nie, *Biomaterials*, 2011, **32**, 1611–1618.

15 L. Zhang, L. Laug, W. Münchgesang, E. Pippel, U. Gösele, M. Brandsch and M. Knez, *Nano Lett.*, 2010, **10**, 219–223.

16 G. Bardi, L. Boselli and P. P. Pompa, *Nanoscale*, 2023, **15**, 14284–14300.

17 A. Clark, A. Zhu, K. Sun and H. R. Petty, *J. Nanopart. Res.*, 2011, **13**, 5547–5555.

18 T. Masuda, H. Fukumitsu, K. Fugane, H. Togasaki, D. Matsumura, K. Tamura, Y. Nishihata, H. Yoshikawa, K. Kobayashi, T. Mori and K. Uosaki, *J. Phys. Chem. C*, 2012, **116**, 10098–10102.

19 S. Gatla, D. Aubert, V. Flaud, R. Grosjean, T. Lunkenbein, O. Mathon, S. Pascarelli and H. Kaper, *Catal. Today*, 2019, **333**, 105–112.

20 A. TROVARELLI, *Catal. Rev.*, 1996, **38**, 439–520.

21 B. Harrison, A. F. Diwell and C. Hallett, *Platinum Met. Rev.*, 1988, **32**, 73–83.

22 B. Ma, J. Han, Q. Zhao, B. Jiang, Z. Zhang, B. Zhao, Z. Liang, Y. Zhang and L. Zhang, *ACS Sustain. Chem. Eng.*, 2023, **11**, 6163–6172.

23 R. Yan, S. Sun, J. Yang, W. Long, J. Wang, X. Mu, Q. Li, W. Hao, S. Zhang, H. Liu, Y. Gao, L. Ouyang, J. Chen, S. Liu, X.-D. Zhang and D. Ming, *ACS Nano*, 2019, **13**, 11552–11560.

24 Z. Li, X. Yang, Y. Yang, Y. Tan, Y. He, M. Liu, X. Liu and Q. Yuan, *Chem. –A Eur. J.*, 2018, **24**, 409–415.

25 F. Bonet, V. Delmas, S. Grugeon, R. Herrera Urbina, P.-Y. Silvert and K. Tekaia-Elhsissen, *Nanostruct. Mater.*, 1999, **11**, 1277–1284.

26 N. V. Long, N. D. Chien, T. Hayakawa, T. Matsubara, M. Ohtaki and M. Nogami, *J. Exp. Nanosci.*, 2012, **7**, 133–149.

27 R. J. Isaifan, S. Ntais and E. A. Baranova, *Appl. Catal., A*, 2013, **464–465**, 87–94.

28 Y. Xue, Q. Luan, D. Yang, X. Yao and K. Zhou, *J. Phys. Chem. C*, 2011, **115**, 4433–4438.

29 Y. Hu, Y. Li, J. He, T. Liu, K. Zhang, X. Huang, L. Kong and J. Liu, *J. Environ. Manage.*, 2018, **226**, 256–263.

30 C. S. Wei, W. Y. Huang, R. J. Zhang, Y. H. Wang, L. M. Luo, H. Mo and L. H. Xiao, *Appl. Mech. Mater.*, 2014, **675–677**, 395–400.

31 S. Yu, Y. Cui, X. Guo, S. Chen, H. Sun, L. Wang, J. Wang, Y. Zhao and Z. Liu, *New J. Chem.*, 2019, **43**, 8774–8780.

32 H. Issa Hamoud, G. Finqueneisel and B. Azambre, *J. Environ. Manage.*, 2017, **195**, 195–207.

33 N. Zhang, J. Chen, Z. Fang and E. P. Tsang, *Chem. Eng. J.*, 2019, **369**, 588–599.

34 S. Ben Hammouda, F. Zhao, Z. Safaei, I. Babu, D. L. Ramasamy and M. Sillanpää, *Appl. Catal., B*, 2017, **218**, 119–136.

35 B. Jain, A. K. Singh, A. Hashmi, M. A. B. H. Susan and J.-P. Lellouche, *Adv. Compos. Hybrid Mater.*, 2020, **3**, 430–441.

36 A. Strzepa, K. A. Pritchard and B. N. Dittel, *Cell. Immunol.*, 2017, **317**, 1–8.

37 J. M. Pullar, M. C. M. Vissers and C. C. Winterbourn, *IUBMB Life*, 2000, **50**, 259–266.

38 N. Kishimoto, *J. Water Environ. Nanotechnol.*, 2019, **17**, 302–335.

39 A. B. Shcherbakov, V. K. Ivanov, T. V Sirota and Y. D. Tret'yakov, *Dokl. Chem.*, 2011, **437**, 60–62.

40 V. K. Klochkov, A. V Grigorova, O. O. Sedyh and Y. V Malyukin, *Colloids Surf., A*, 2012, **409**, 176–182.

41 B. Ballantyne and W. M. Snellings, *J. Appl. Toxicol.*, 2007, **27**, 291–299.

42 Z. Zhu, Z. Wang, C. Zhang, Y. Wang, H. Zhang, Z. Gan, Z. Guo and X. Wang, *Chem. Sci.*, 2019, **10**, 3089–3095.

43 S. J. Dixon, K. M. Lemberg, M. R. Lamprecht, R. Skouta, E. M. Zaitsev, C. E. Gleason, D. N. Patel, A. J. Bauer, A. M. Cantley, W. S. Yang, B. Morrison III and B. R. Stockwell, *Cell*, 2012, **149**, 1060–1072.

44 J. Lewerenz, G. Ates, A. Methner, M. Conrad and P. Maher, *Front. Neurosci.*, 2018, **12**, 214.

45 S. J. Dixon, D. N. Patel, M. Welsch, R. Skouta, E. D. Lee, M. Hayano, A. G. Thomas, C. E. Gleason, N. P. Tatonetti, B. S. Slusher and B. R. Stockwell, *Elife*, 2014, **3**, e02523.

46 Y. Zhang, S. Liu, J. Peng, S. Cheng, Q. Zhang, N. Zhang, Z. Zhou, Y. Zhang, Y. Zhao and T. Liu, *Nutrients*, 2023, **15**, 1090.

47 W. Strober, *Curr. Protoc. Immunol.*, 2015, **111**, B1–B3.

48 D. Dupkalová, Y. Kosto, V. Kalinovych, A. Deineko, S. Franchi, J. Nováková, I. Matolínová, T. Skála, K. C. Prince, A. Fučíková, A. B. Shcherbakov, N. M. Zholobak and N. Tsud, *Appl. Surf. Sci.*, 2023, **636**, 157793.